Published in final edited form as:

Mol Pharm. 2019 April 01; 16(4): 1694–1702. doi:10.1021/acs.molpharmaceut.9b00025.

Evaluation of A Novel Pb-203-Labeled Lactam-Cyclized Alpha-Melanocyte-Stimulating Hormone Peptide for Melanoma Targeting

Jianquan Yang[†], **Jingli Xu**[†], **Lina Cheuy**[†], **Rene Gonzalez**[‡], **Darrell R. Fisher**[§], and **Yubin Miao**[†]

[†]Department of Radiology, University of Colorado Denver, Aurora, CO 80045, USA.

[‡]Department of Medical Oncology, University of Colorado Denver, Aurora, CO 80045, USA.

[§]Versant Medical Physics and Radiation Safety, Richland, WA 99354, USA.

Abstract

The purpose of this study is to examine the melanocortin-1 receptor (MC1R) targeting and specificity of ^{203}Pb-DOTA-GGNle-CycMSH$_{hex}$ in melanoma cells and tumors to facilitate its potential therapeutic application when labeled with ^{212}Pb. The melanocortin-1 receptor (MC1R)-specific targeting and imaging properties of ^{203}Pb-DOTA-GGNle-CycMSH$_{hex}$ were determined on B16/F1 and B16/F10 murine melanoma cells, and in B16/F1 flank melanoma-, B16/F10 flank melanoma- and B16/F10 pulmonary metastatic melanoma-bearing C57 mice. ^{203}Pb-DOTA-GGNle-CycMSH$_{hex}$ displayed MC1R-specific binding on B16/F1 and B16/F10 melanoma cells and tumors. B16/F1 flank melanoma, B16/F10 flank melanoma and B16/F10 pulmonary metastatic melanoma lesions could be clearly imaged by single photon emission computed tomography (SPECT) using ^{203}Pb-DOTA-GGNle-CycMSH$_{hex}$ as an imaging probe. The favorable melanoma targeting and imaging properties highlighted the potential of ^{203}Pb-DOTA-GGNle-CycMSH$_{hex}$ as a MC1R-targeting melanoma imaging probe, and warranted the evaluation of ^{212}Pb-DOTA-GGNle-CycMSH$_{hex}$ for melanoma therapy in future studies.

Graphical Abstract

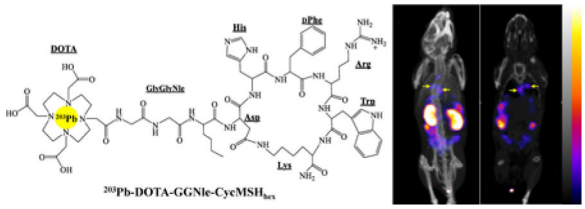

Keywords

Melanocortin-1 receptor; ^{203}Pb-DOTA-GGNle-CycMSH$_{hex}$; Single photon emission computed tomography; Melanoma imaging

Corresponding Author: Yubin Miao, 12700 East 19th Ave., MS C278, Department of Radiology, School of Medicine, University of Colorado Denver, Aurora, CO 80045, USA. Phone: (303) 724-3763; yubin.miao@ucdenver.edu.

INTRODUCTION

Malignant melanoma is the most deadly skin cancer with an increasing incidence. Approximately 91,270 new cases and 9,320 deaths will occur in the United States in 2018.[1] Malignant melanoma accounts for 75% of all skin cancer deaths despite that melanoma is only less than 5% of skin cancer cases.[1] High mortality of melanoma is attributed to the extreme aggressiveness associated with metastatic melanoma. Traditional median overall survival is about 6–9 months for metastatic melanoma patients.[2, 3] Although new treatments including Vemurafenib (BRAF inhibitor), ipilimumab (targeting CTLA-4) and Nivolumab (PD-1 inhibitor) have improved median overall survivals of metastatic melanoma patients by months,[4–8] the long-term survival remains less than 10% for metastatic melanoma patients. Therefore, there is a need to develop new approaches to treatmetastatic melanoma.

Due to the over-expression of melanocortin-1 receptors (MC1Rs) on more than 80% of melanotic and amelanotic human melanoma metastases,[9–14] we have been developing radiolabeled alpha-melanocyte-stimulating hormone (α-MSH) peptides to target MC1Rs for melanoma imaging and therapy. Our radiolabeled lactam-cyclized α-MSH peptides, building upon the structure of DOTA-GGNle-CycMSH$_{hex}$ {1,4,7,10-tetraazacyclononane-1,4,7,10-tetraacetic acid-Gly-Gly-Nle-c[Asp-His-DPhe-Arg-Trp-Lys]-CONH$_2$},[15–23] were readily radiolabeled with both single photon emission tomography (SPECT) radionuclides (i.e. ^{111}In and ^{67}Ga)[16, 19] and positron emission tomography (PET) radionuclides (i.e. ^{64}Cu and ^{68}Ga)[20, 23] for melanoma detection, and ^{177}Lu for potential treatment of melanoma using targeted radionuclide.[21]

^{177}Lu-DOTA-GGNle-CycMSH$_{hex}$ displayed promising melanoma targeting property in B16/F1 melanoma-bearing mice.[21] Thus we are interested in replacing ^{177}Lu with matched-pair theranostic radionuclides ^{203}Pb/^{212}Pb due to their attractive decay properties. ^{203}Pb is a cyclotron-produced radionuclide with 51.9 h half-life. It generates a 279 keV gamma ray with 81% abundance which is suitable for SPECT imaging. ^{212}Pb ($T_{1/2}$ = 10.6 h) can be easily obtained from a ^{224}Ra-^{212}Pb generator. ^{212}Pb decays to ^{212}Bi via a beta-decay (0.57 MeV), then ^{212}Bi eventually decays to stable ^{208}Pb through two beta-decays (1.8 and 2.2 MeV) and two alpha-decays (6.1 and 8.8 MeV). Therefore, ^{212}Pb can serve as an in vivo generator that can be delivered by MC1R-binding DOTA-GGNle-CycMSH$_{hex}$ peptide. Moreover, ^{203}Pb/^{212}Pb share identical radiolabeling chemistry. Thus, the radiolabeling of ^{203}Pb/^{212}Pb can be conducted under identical radiolabeling conditions. The combination of ^{203}Pb/^{212}Pb-DOTA-GGNle-CycMSH$_{hex}$ could potentially open the avenue for imaging-guided alpha radionuclide therapy by identifying MC1R-positive melanoma patients.

In this study, DOTA-GGNle-CycMSH$_{hex}$ was prepared using fluorenylmethyloxycarbonyl (Fmoc) chemistry and radiolabeled with ^{203}Pb. The specific binding of ^{203}Pb-DOTA-GGNle-CycMSH$_{hex}$ was determined on B16/F1 and B16/F10 murine melanoma cells. The selection of B16/F1 and B16/F10 cells for this study was based on two reasons. First, B16/F1 murine melanoma cells are commonly used by research groups to generate flank melanoma-bearing miceto evaluate the melanoma targeting and biodistribution properties of radiolabeled α-MSH peptides.[12, 15, 16] Second, B16/F10 murine melanoma cells are highly

metastatic and thus are used to generate pulmonary melanoma metastases by tail vein injection of cells.[14, 24, 25] Hence, we generated B16/F1 flank melanoma-, B16/F10 flank melanoma- and B16/F10 pulmonary metastatic melanoma-bearing C57 mice to determine the tumor targeting and biodistribution of ^{203}Pb-DOTA-GGNle-CycMSH$_{hex}$ in this study. Thereafter, the biodistribution and imaging properties of ^{203}Pb-DOTA-GGNle-CycMSH$_{hex}$ were examined using B16/F1 flank melanoma-, B16/F10 flank melanoma- and pulmonary metastatic melanoma-bearing mice.

EXPERIMENTAL SECTION

Chemicals and reagents

Amino acids and resin were purchased from Advanced ChemTech Inc. (Louisville, KY) and Novabiochem (San Diego, CA). DOTA-tri-t-butyl ester was purchased from Macrocyclics Inc. (Richardson, TX) for peptide synthesis. $^{203}PbCl_2$ was purchased from Lantheus Medical Imaging (North Billerica, MA) for radiolabeling. All other chemicals used in this study were purchased from Thermo Fisher Scientific (Waltham, MA) and used without further purification. B16/F1 and B16/F10 murine melanoma cells were obtained from American Type Culture Collection (Manassas, VA).

Preparation of ^{203}Pb-DOTA-GGNle-CycMSH$_{hex}$ and its serum stability and urine metabolites

DOTA-GGNle-CycMSH$_{hex}$ was synthesized using standard fluorenylmethyloxycarbonyl (Fmoc) chemistry according to our published procedure.[16] The peptide was purified by reverse phase-high performance liquid chromatography (RP-HPLC) and characterized by liquid chromatography-mass spectrometry (LC-MS). ^{203}Pb-DOTA-GGNle-CycMSH$_{hex}$ was prepared in a 0.25 M NH_4OAc-buffered solution (pH 5.3). Briefly, 50 μL of $^{203}PbCl_2$ (37–74 MBq in 0.5 M HCl aqueous solution), 10 μL of peptide aqueous solution (1 mg/mL) and 300 μL of 0.25 M NH_4OAc were added into a reaction vial and incubated at 75 °C for 30 min. After the reaction, 10 μL of 0.5% EDTA (ethylenediaminetetraacetic acid) aqueous solution was added into the reaction vial to scavenge potential unbound $^{203}Pb^{2+}$ ions. The radiolabeled complexes were purified to single species by Waters RP-HPLC (Milford, MA) on a Grace Vydac C-18 reverse phase analytical column (Deerfield, IL) using the following gradient at a 1 mL/min flowrate. The mobile phase included 20 mM HCl aqueous solution as solvent A () and 100% CH_3CN as solvent B. The gradient was initiated and kept at 82:18 A/B for 3 min followed by a linear gradient of 82:18 A/B to 72:28 A/B over 20 min. Thereafter, the gradient was changed from 72:28 A/B to 10:90 A/B over 3 min followed by an additional 5 min at 10:90 A/B. Then the gradient was changed from 10:90 A/B to 82:18 A/B over 3 min. The purified peptide sample was purged with N_2 gas to remove the acetonitrile for 15 min. The pH of the final solution was adjusted to 7.4 using 0.1 N NaOH and sterile saline for animal studies. ^{203}Pb-DOTA-GGNle-CycMSH$_{hex}$ was incubated in mouse serum at 37 °C for 4 h and monitored for degradation by RP-HPLC to determine its *in vitro* serum stability. Furthermore, one hundred microliter of HPLC-purified ^{203}Pb-DOTA-GGNle-CycMSH$_{hex}$ (0.74 MBq) was injected into a normal C57 mouse through the tail vein to determine urine metabolites.. The mouse was sacrificed at 2 h post-injection and the urine was collected. The radioactive urine metabolites were analyzed by injecting

aliquots of urine into HPLC. A 20-minute gradient of 18–28% acetonitrile / 20 mM HCl was used to analyze the urine metabolites.

Specific cellular binding, internalization and efflux of ^{203}Pb-DOTA-GGNle-CycMSH$_{hex}$

The specific binding of ^{203}Pb-DOTA-GGNle-CycMSH$_{hex}$ was determined on B16/F1 and B16/F10 melanoma cells. The B16/F1 and B16/F10 cells (1×10^6 cells pertube, n = 3) were incubated at 25 °C for 2 h with approximately 0.037 MBq of ^{203}Pb-DOTA-GGNle-CycMSH$_{hex}$ with or without 10 μg (6.07 nmol) of unlabeled [Nle^4, D-Phe^7]-α-MSH (NDP-MSH) in 0.3 mL of binding medium {Modified Eagle's medium with 25 mM *N*-(2-hydroxyethyl)-piperazine-*N*'-(2-ethanesulfonic acid), pH 7.4, 0.2% bovine serum albumin (BSA), 0.3 mM 1,10-phenathroline}. The binding medium was aspirated after the incubation. The cells were rinsed three times with 0.5 ml of ice-cold pH 7.4, 0.2% BSA/0.01 M phosphate buffered saline (PBS) and measured in a Wallac 1480 automated gamma counter (PerkinElmer, NJ).

The internalization and efflux properties of ^{203}Pb-DOTA-GGNle-CycMSH$_{hex}$ were examined on B16/F1 and B16/F10 melanoma cells. B16/F1 or B16/F10 cells (3×10^5/well) were seeded into a 24-well cell culture plate and incubated at 37°C overnight. After being washed once with binding media (MEM with 25 mM HEPES, pH 7.4, 0.2% BSA, 0.3 mM 1,10-phenathroline), the cells were incubated at 25°C for 20, 40, 60, 90 and 120 min (n = 3) with approximately 100,000 counts per minute (cpm) of HPLC-purified ^{203}Pb-DOTA-GGNle-CycMSH$_{hex}$. After incubation, the reaction medium was aspirated and cells were rinsed with 2 × 0.5 mL of ice-cold pH 7.4, 0.2% BSA / 0.01 M PBS. Cellular internalization of ^{203}Pb-DOTA-GGNle-CycMSH$_{hex}$ was evaluated by washing the cells with acidic buffer [40 mM sodium acetate (pH 4.5) containing 0.9% NaCl and 0.2% BSA] to remove the membrane bound radioactivity. The remaining internalized radioactivity was obtained by lysing the cells with 0.5 mL of 1N NaOH for 5 min. Membrane-bound and internalized ^{203}Pb activity was counted in a gamma counter. Cellular efflux of ^{203}Pb-DOTA-GGNle-CycMSH$_{hex}$ was determined by incubating cells with ^{203}Pb-DOTA-GGNle-CycMSH$_{hex}$ at 25 °C for 2 h, removing non-specific bound activity with 2 × 0.5 mL of ice-cold pH 7.4, 0.2% BSA / 0.01 M PBS rinse, and monitoring radioactivity released into cell culture media.The radioactivity in media, on cell surfaces and in cells were separately collected and counted in a gamma counter 20, 40, 60, 90 and 120 min post incubation.

B16/F1 and B16/F10 melanoma-bearing mice for biodistribution and imaging studies

All animal studies were performed in compliance with Institutional Animal Care and Use Committee approval. B16/F1 flank melanoma-, B16/F10 flank melanoma- and pulmonary metastatic melanoma-bearing mice were generated for biodistribution and imaging studies. bearing mice Each C57 mouse was subcutaneously inoculated with 1×10^6 B16/F1 or B16/F10 cells on the right flank to generate flank tumors. The flank tumor weights reached approximately 0.2 g after 10 days and the tumor-bearing mice were used for biodistribution and imaging studies. To generate B16/F10 pulmonary melanoma metastases, each C57 mouse was intravenously injected with 2×10^5 B16/F10 cells into the tail vein. The mice were used for biodistribution and imaging studies 16 days post-injection.

Biodistribution and imaging studies of ^{203}Pb-DOTA-GGNle-CycMSH$_{hex}$

The biodistribution property of ^{203}Pb-DOTA-GGNle-CycMSH$_{hex}$ were determined on B16/F1 flank melanoma-, B16/F10 flank melanoma- and pulmonary metastatic melanoma-bearing C57 mice (Charles River, Wilmington, MA). Each tumor-bearing mouse was injected with 0.056 MBq of ^{203}Pb-DOTA-GGNle-CycMSH$_{hex}$ through the tail vein. Tumor-bearing mice were sacrificed at 0.5, 2, 4 and 24 h post-injection. Tumors and organs of interest were collected, weighed and counted. Blood values were calculated as 6.5% of the whole-body weight. The specificity of the tumor uptake of ^{203}Pb-DOTA-GGNle-CycMSH$_{hex}$ was examined by co-injecting 10 μg (6.07 nmol) of unlabeled NDP-MSH peptide.

Flank melanoma- and pulmonary metastatic melanoma-bearing mice were used to determine the melanoma imaging property of ^{203}Pb-DOTA-GGNle-CycMSH$_{hex}$. Each tumor-bearing mouse was injected with 7.4 MBq of ^{203}Pb-DOTA-GGNle-CycMSH$_{hex}$ through the tail vein. SPECT imaging studies were performed at 2 h post-injection. CT data was collected followed by SPECT data acquisition. Reconstructed SPECT/CT data were visualized using Vivoquant (Invicro, Boston, MA).

Statistical Analysis

Student's t-test for unpaired data was performed for statistical analysis. A 95% confidence level was chosen to determine the difference between groups in cellular binding of ^{203}Pb-DOTA-GGNle-CycMSH$_{hex}$, difference in tumor and kidney uptake between ^{203}Pb-DOTA-GGNle-CycMSH$_{hex}$ with/without NDP-MSH blockade, and the difference in lung uptake in normal lung and metastatic melanoma-bearing lung. The differences at the 95% confidence level ($p<0.05$) were considered significant.

RESULTS

DOTA-GGNle-CycMSH$_{hex}$ (Fig. 1) was synthesized and purified by reverse phase high pressure liquid chromatography (RP-HPLC) and displayed greater than 90% purity after HPLC purification. The identity of DOTA-GGNle-CycMSH$_{hex}$ was confirmed by electrospray ionization mass spectrometry. ^{203}Pb-DOTA-GGNle-CycMSH$_{hex}$ was readily prepared with greater than 95% radiolabeling yield, and was completely separated from its excess non-labeled peptide by RP-HPLC. The retention time of ^{203}Pb-DOTA-GGNle-CycMSH$_{hex}$ was 18.3 min. ^{203}Pb-DOTA-GGNle-CycMSH$_{hex}$ was stable in mouse serum at 37 °C for 4 h. The urine analysis revealed that approximately 65% of ^{203}Pb-DOTA-GGNle-CycMSH$_{hex}$ remained intact in urine at 2 h post-injection (Fig. 2). ^{203}Pb-DOTA-GGNle-CycMSH$_{hex}$ displayed MC1R-specific binding on B16/F1 and B16/F10 cells. Approximately 79% and 84% of ^{203}Pb-DOTA-GGNle-CycMSH$_{hex}$ uptake were blocked by peptide blockade on B16/F1 and B16/F10 cells ($p<0.05$).

Figure 3 illustrates the internalization and efflux of ^{203}Pb-DOTA-GGNle-CycMSH$_{hex}$ on B16/F1 and B16/F10 cells. ^{203}Pb-DOTA-GGNle-CycMSH$_{hex}$ exhibited rapid cellular internalization property on B16/F1 cells. Approximately 52% and 62% of ^{203}Pb-DOTA-GGNle-CycMSH$_{hex}$ activity were internalized in the B16/F1 cells after 40 min and 2 h

incubation, respectively. Cellular efflux of ^{203}Pb-DOTA-GGNle-CycMSH$_{hex}$ demonstrated that 90% and 80% of the ^{203}Pb activity remained inside the B16/F1 cells 40 min and 2 h after incubating cells in culture medium at 25 °C, respectively. ^{203}Pb-DOTA-GGNle-CycMSH$_{hex}$ exhibited similar internalization and efflux patterns on B16/F10 cells. Approximately 48% and 67% of ^{203}Pb-DOTA-GGNle-CycMSH$_{hex}$ activity were internalized in the B16/F10 cells after 40 min and 2 h incubation, respectively. Cellular efflux of ^{203}Pb-DOTA-GGNle-CycMSH$_{hex}$ indicated that 96% and 91% of the ^{203}Pb activity remained inside the B16/F10 cells 40 min and 2 h after cell incubation in culture medium at 25 °C, respectively.

The tumor targeting and biodistribution properties of ^{203}Pb-DOTA-GGNle-CycMSH$_{hex}$ were determined on B16/F1 flank melanoma-, B16/F10 flank melanoma- and pulmonary metastatic melanoma-bearing C57 mice. The biodistribution results of ^{203}Pb-DOTA-GGNle-CycMSH$_{hex}$ are presented in Tables 1–3. The B16/F1 tumor uptake was 14.37 ± 3.43 and 12.61 ± 2.28% ID/g at 0.5 and 2 h post-injection, respectively. ^{203}Pb-DOTA-GGNle-CycMSH$_{hex}$ exhibited prolonged B16/F1 tumor retention, with 9.37 ± 2.23 and 6.4 ± 0.37% ID/g at 4 and 24 h post-injection, respectively. The co-injection of non-radioactive NDP-MSH blocked 94% of the B16/F1 tumor uptake at 2 h post-injection, demonstrating that the B16/F1 tumor uptake was MC1R-mediated. Whole-body clearance of ^{203}Pb-DOTA-GGNle-CycMSH$_{hex}$ was rapid, with approximately 92% of the injected dose being washed out of the body via urinary system by 2 h post-injection. Kidneys are the normal organs with the highest uptake of ^{203}Pb-DOTA-GGNle-CycMSH$_{hex}$. The renal uptake was 9.3 ± 1.75, 4.99 ± 1.48 and 4.82 ± 0.59% ID/g at 0.5, 2 and 4 h post-injection, respectively, and decreased to 2.77 ± 0.81% ID/g at 24 h post-injection. The co-injection of NDP-MSH didn't significantly decrease the renal uptake ($p>0.05$), suggesting that the renal uptake of ^{203}Pb-DOTA-GGNle-CycMSH$_{hex}$ was not receptor-specific. The accumulation of ^{203}Pb-DOTA-GGNle-CycMSH$_{hex}$ in other normal organs was much lower than kidneys. ^{203}Pb-DOTA-GGNle-CycMSH$_{hex}$ displayed high tumor/blood and tumor/normal organ uptake ratios as early as 0.5 h post-injection.

^{203}Pb-DOTA-GGNle-CycMSH$_{hex}$ displayed similar uptake in B16/F10 flank melanoma as the uptake in B16/F1 flank melanoma. The B16/F10 tumor uptake was 11.29 ± 4.42, 16.81 ± 5.48, 12.67 ± 1.48, 4.57 ± 2.17% ID/g at 0.5, 2, 4 and 24 h post-injection, respectively. The co-injection of non-radioactive NDP-MSH blocked 95% of the B16/F10 tumor uptake at 2 h post-injection, demonstrating that the tumor uptake was MC1R-specific. ^{203}Pb-DOTA-GGNle-CycMSH$_{hex}$ exhibited similar urinary clearance pattern in B16/F10 and B16/F1 flank melanoma-bearing mice. The kidney uptake was 12.9 ± 4.98, 5.43 ± 2.0 and 5.31 ± 1.1% ID/g in B16/F10 flank melanoma-bearing mice at 0.5, 2 and 4 h post-injection, respectively. The renal uptake gradually decreased to 3.87 ± 2.12% ID/g at 24 h post-injection. Similarly, the co-injection of NDP-MSH didn't significantly reduce the renal uptake ($p>0.05$), indicating that the renal uptake of ^{203}Pb-DOTA-GGNle-CycMSH$_{hex}$ was not receptor-specific. Because of low accumulation in other normal organs, ^{203}Pb-DOTA-GGNle-CycMSH$_{hex}$ exhibited high tumor/blood and tumor/normal organ uptake ratios as early as 0.5 h post-injection.

As shown in Table 3, ^{203}Pb-DOTA-GGNle-CycMSH$_{hex}$ exhibited rapid uptake in pulmonary metastatic melanoma-bearing lung. The uptake in metastatic melanoma-bearing lung was 7.32 ± 2.13, 9.27 ± 1.13 and 3.9 ± 0.18% ID/g at 2, 4 and 24 h post-injection, respectively. The uptake in metastatic melanoma-bearing lung was 13–33 times the uptake of normal lung. ^{203}Pb-DOTA-GGNle-CycMSH$_{hex}$ displayed similar accumulation pattern in normal organs of pulmonary metastatic melanoma-bearing mice as compared to the accumulation in normal organs of flank melanoma-bearing mice. The representative maximum intensity projection SPECT images in flank melanoma- and pulmonary metastatic melanoma-bearing mice are presented in Figure 4. Both B16/F1 and B16/F10 flank melanoma lesions could be visualized by SPECT using ^{203}Pb-DOTA-GGNle-CycMSH$_{hex}$ as an imaging probe at 2 h post-injection. Moreover, the pulmonary melanoma metastases could be clearly imaged by SPECT using ^{203}Pb-DOTA-GGNle-CycMSH$_{hex}$ as an imaging probe at 2 h post-injection.

DISCUSSION

We have been developing MC1R-targeting α-MSH peptide radiopharmaceuticals for melanoma imaging and therapy because of the expression of MC1Rs on both melanotic and amelanotic human melanoma metastases.[9] Our recent first-in-human images of melanoma metastases in clearly demonstrated the clinical relevance of MC1R as a molecular target for human melanoma imaging.[23] The melanoma metastases in brain, lung, connective tissue and small intestine of patients could be clearly visualized by positron emission tomography (PET) using ^{68}Ga-DOTA-GGNle-CycMSH$_{hex}$ as an imaging probe.[23] The remarkable PET images of melanoma metastases in patients highlighted the need to develop MC1R-targeting therapeutic peptide for treating patients with melanoma metasases. Therefore, we have committed efforts to develop ^{203}Pb/^{212}Pb-DOTA-GGNle-CycMSH$_{hex}$ peptides for potential imaging-guided melanoma therapy because of the attractive theranostic properties of matched-pair ^{203}Pb/^{212}Pb and nanomolar MC1R binding affinity of DOTA-GGNle-CycMSH$_{hex}$ with B16/F1 and B16/F10 melanoma cells.[16, 23] In this study, we prepared ^{203}Pb-DOTA-GGNle-CycMSH$_{hex}$ and evaluated its MC1R binding specificity with melanoma cells, and its melanoma targeting and imaging properties in flank melanoma-bearing and pulmonary metastatic melanoma-bearing mice.

^{203}Pb-DOTA-GGNle-CycMSH$_{hex}$ displayed MC1R-specific binding on B16/F1 and B16/F10 melanoma cells. The biodistribution and imaging properties of ^{203}Pb-DOTA-GGNle-CycMSH$_{hex}$ were examined in B16/F1 flank melanoma-, B16/F10 flank melanoma- and B16/F10 pulmonary metastatic melanoma-bearing micebecause these melanoma models have been used among research groups to evaluate the tumor targeting properties of radiolabeled α-MSH peptides.[14, 18, 24–30] ^{203}Pb-DOTA-GGNle-CycMSH$_{hex}$ exhibited similar MC1R-specific uptake in B16/F1 and B16/F10 melanoma lesions. The phantom imaging of $^{99m}TcO_4^-$ and $^{203}PbCl_2$ exhibited comparable tomographic spatial resolution of 1.6 mm[31] and highlighted the SPECT imaging potential of ^{203}Pb. In this study, B16/F1 flank melanoma, B16/F10 flank melanoma and B16/F10 pulmonary metastatic melanoma lesions could be clearly imaged by SPECT using ^{203}Pb-DOTA-GGNle-CycMSH$_{hex}$ as an imaging probe.

^{203}Pb can be produced by irradiating natural or enriched ^{203}Tl and ^{205}Tl targets with 13.7-MeV deuterons through a ^{203}Tl (d, 2n) ^{203}Pb reaction,[32] 14.5-MeV protons through a ^{203}Tl (p, n) ^{203}Pb reaction,[33] and 26.5-MeV protons through a ^{205}Tl (p, 3n) ^{203}Pb reaction.[34] Non-radioactive Pb and Fe are the major metallic contaminants in the $^{203}PbCl_2$ solution produced by the ^{205}Tl (p, 3n) ^{203}Pb reaction, thus serve as competitors for ^{203}Pb in the radiolabeling process. The amount of non-radioactive Pb varies from 0.15 to 0.65 μg/mCi, whereas the amount of non-radioactive Fe ranges from 0.1 to 0.19 μg/mCi. Therefore, excess amount of DOTA-GGNle-CycMSH$_{hex}$ was used for radiolabeling. Despite that HPLC purification completely separated DOTA-GGNle-CycMSH$_{hex}$ from ^{203}Pb-DOTA-GGNle-CycMSH$_{hex}$, HPLC purification couldn't get rid of non-radioactive Pb- and Fe-labeled peptides that could compete with ^{203}Pb-DOTA-GGNle-CycMSH$_{hex}$ for MC1R receptors in melanoma lesions. Therefore, in order to minimize the competition of MC1Rs from non-radioactive Pb- and Fe-labeled peptides, it is desirable to improve the specific activity of ^{203}Pb during the production and processing.

Non-radioactive Re-cyclized ^{203}Pb-DOTA-Re(Arg^{11})CCMSH displayed high MC1R-specific uptake (12 ± 3.2% ID/g at 1 h post-injection) in B16/F10 melanoma.[31] B16/F1 flank melanoma was clearly visualized by SPECT using ^{203}Pb-DOTA-Re(Arg^{11})CCMSH as an imaging probe.[31] In this study, ^{203}Pb-DOTA-GGNle-CycMSH$_{hex}$ exhibited similar B16/F1 tumor uptake (14.37 ± 3.43% ID/g at 0.5 h post-injection) and renal uptake (4.99 ± 1.48% ID/g at 2 h post-injection) as compared to ^{203}Pb-DOTA-Re(Arg^{11})CCMSH. Importantly, the pulmonary metastatic melanoma lesions could be clearly identified by SPECT using ^{203}Pb-DOTA-GGNle-CycMSH$_{hex}$ as an imaging probe in this study, suggesting the potential utilization of ^{203}Pb-DOTA-GGNle-CycMSH$_{hex}$ to identify melanoma patients with MC1R-positive tumors for MC1R-targeted radionuclide therapy.

The statistical analysis of tumor and renal uptake of ^{203}Pb/^{212}Pb-DOTA-Re(Arg^{11})CCMSH demonstrated the matched-pair properties of ^{203}Pb/^{212}Pb.[31, 35] Moreover, ^{212}Pb-DOTA-Re(Arg^{11})CCMSH exhibited remarkable dose-dependent therapeutic efficacy in extremely aggressive B16/F1 melanoma model. For instance, 20% and 45% of the mice receiving 100 or 200 μCi of ^{212}Pb-DOTA-Re(Arg^{11})CCMSH survived the 120-d study disease free.[35] Interestingly, ^{203}Pb-DOTA-GGNle-CycMSH$_{hex}$ displayed comparable B16/F1 tumor uptake and renal uptake in this study. According to the matched-pair melanoma targeting properties of ^{203}Pb/^{212}Pb-DOTA-Re(Arg11)CCMSH,[31, 35] we anticipate that ^{212}Pb-DOTA-GGNle-CycMSH$_{hex}$ would exhibit similar melanoma uptake and biodistribution profile as ^{203}Pb-DOTA-Re(Arg^{11})CCMSH in same melanoma model. Favorable tumor targeting and pharmacokinetic properties of ^{203}Pb-DOTA-GGNle-CycMSH$_{hex}$ warranted the further evaluation of ^{212}Pb-DOTA-GGNle-CycMSH$_{hex}$. It would be interesting to determine the biodistribution property and therapeutic efficacy of ^{212}Pb-DOTA-GGNle-CycMSH$_{hex}$ in the future.

In summary, ^{203}Pb-DOTA-GGNle-CycMSH$_{hex}$ exhibited MC1R-targeting and specificity on B16/F1 and B16/F10 melanoma cells and tumors. B16/F1 flank melanoma, B16/F10 flank melanoma and B16/F10 pulmonary metastatic melanoma lesions could be clearly imaged by SPECT using ^{203}Pb-DOTA-GGNle-CycMSH$_{hex}$ as an imaging probe. The favorable melanoma targeting and imaging properties highlighted the potential of ^{203}Pb-DOTA-

GGNle-CycMSH$_{hex}$ as a MC1R-targeting melanoma imaging probe, and warranted the evaluation of ^{212}Pb-DOTA-GGNle-CycMSH$_{hex}$ for melanoma therapy in future studies.

ACKNOWLEDGMENTS

We thank Drs. Fabio Gallazzi and Michael Schultz for their technical assistance. This work was supported in part by the NIH grant R01CA225837 and University of Colorado Denver start-up fund.

ABBREVIATIONS USED

α-MSH	α-melanocyte stimulating hormone
MC1R	melanocortin-1 receptor
SPECT	single photon emission computed tomography
PET	positron emission tomography
Fmoc	fluorenylmethyloxycarbonyl
RP-HPLC	reverse phase-high performance liquid chromatography
LC-MS	liquid chromatography-mass spectrometry
DAPI 4'	6-diamidino-2-phenylindole
EDTA	ethylenediaminetetraacetic acid
NDP-MSH	[Nle^4, D-Phe^7]-α-MSH
BSA	bovine serum albumin
PBS	phosphate buffered saline
MEM	Modified Eagle's medium

REFERENCES

1. Siegel RL, Miller KD, Jemal A. Cancer Statistics, 2018. CA Cancer J. Clin 2018, 68, 7–30. [PubMed: 29313949]
2. Tsao H, Atkins MB, Sober AJ. Management of cutaneous melanoma. N. Engl. J. Med 2004, 54, 8–29.
3. Atallah E, Flaherty L. Treatment of metastatic malignant melanoma. Curr. Treat. Options Oncol 2005, 6, 185–193. [PubMed: 15869730]
4. Chapman PB, Hauschild A, Robert C, Haanen JB, Ascierto P, Larkin J, Dummer R, Garbe C, Testori A, Maio M, Hogg D, Lorigan P, Lebbe C, Jouary T, Schadendorf D, Ribas A, O'Day SJ, Sosman JA, Kirkwood JM, Eggermont AM, Dreno B, Nolop K, Li J, Nelson B, Hou J, Lee RJ, Flaherty KT, McArthur GA; BRIM-3 Study Group. Improved survival with vemurafenib in melanoma with BRAF V600E mutation. N. Engl. J. Med 2011, 364, 2507–2516. [PubMed: 21639808]
5. Sosman JA, Kim KB, Schuchter L, Gonzalez R, Pavlick AC, Weber JS, McArthur GA, Hutson TE, Moschos SJ, Flaherty KT, Hersey P, Kefford R, Lawrence D, Puzanov I, Lewis KD, Amaravadi RK, Chmielowski B, Lawrence HJ, Shyr Y, Ye F, Li J, Nolop KB, Lee RJ, Joe AK, Ribas A. Survival in BRAF V600-mutant advanced melanoma treated with vemurafenib. N. Engl. J. Med 2012, 366, 707–714. [PubMed: 22356324]

6. Hodi FS, O'Day SJ, McDermott DF, Weber RW, Sosman JA, Haanen JB, Gonzalez R, Robert C, Schadendorf D, Hassel JC, Akerley W, van den Eertwegh AJ, Lutzky J, Lorigan P, Vaubel JM, Linette GP, Hogg D, Ottensmeier CH, Lebbé C, Peschel C, Quirt I, Clark JI, Wolchok JD, Weber JS, Tian J, Yellin MJ, Nichol GM, Hoos A, Urba WJ. Improved survival with ipilimumab in patients with metastatic melanoma. N. Engl. J. Med 2010, 363, 711–723. [PubMed: 20525992]
7. Weber JS, O'Day S, Urba W, Powderly J, Nichol G, Yellin M, Snively J, Hersh E. Phase I/II study of ipilimumab for patients with metastatic melanoma. J. Clin. Oncol 2008, 26, 5950–5956. [PubMed: 19018089]
8. Topalian SL, Sznol M, McDermott DF, Kluger HM, Carvajal RD, Sharfman WH, Brahmer JR, Lawrence DP, Atkins MB, Powderly JD, Leming PD, Lipson EJ, Puzanov I, Smith DC, Taube JM, Wigginton JM, Kollia GD, Gupta A, Pardoll DM, Sosman JA, Hodi FS. Survival, durable tumor remission, and long-term safety in patients with advanced melanoma receiving nivolumab. J. Clin. Oncol 2014, 32, 1020–1030. [PubMed: 24590637]
9. Tatro JB, Wen Z, Entwistle ML, Atkins MB, Smith TJ, Reichlin S, Murphy JR. Interaction on an α-melanocyte stimulating hormone-diptheria toxin fusion protein with melanotropin receptors in human metastases. Cancer Res 1992, 52, 2545–2548. [PubMed: 1314697]
10. Siegrist W, Solca F, Stutz S, Giuffre L, Carrel S, Girard J, Eberle AN. Characterization of receptors for alpha-melanocyte-stimulating hormone on human melanoma cells. Cancer Res 1989, 49, 6352–6358. [PubMed: 2804981]
11. Tatro JB and Reichlin S. Specific receptors for alpha-melanocyte-stimulating hormone are widely distributed in tissues of rodents. Endocrinology 1987, 121, 1900–1907. [PubMed: 2822378]
12. Chen J, Cheng Z, Hoffman TJ, Jurisson SS, Quinn TP. Melanoma-targeting properties of ^{99m}Technetium-labeled cyclic α-melanocyte-stimulating hormone peptide analogues. Cancer Res 2000, 60, 5649–5658. [PubMed: 11059756]
13. Miao Y, Whitener D, Feng W, Owen NK, Chen J, Quinn TP. Evaluation of the human melanoma targeting properties of radiolabeled alpha-melanocyte stimulating hormone peptide analogues. Bioconjug. Chem 2003, 14, 1177–1184. [PubMed: 14624632]
14. Guo H, Shenoy N, Gershman BM, Yang J, Sklar LA, Miao Y. Metastatic melanoma imaging with an 111In-labeled lactam bridge-cyclized alpha-melanocyte stimulating hormone peptide. Nuc.l Med. Biol 2009, 36, 267–276.
15. Guo H, Yang J, Gallazzi F, Miao Y. Reduction of the ring size of radiolabeled lactam bridge-cyclized alpha-MSH peptide resulting in enhanced melanoma uptake. J. Nucl. Med 2010, 51, 418–426. [PubMed: 20150256]
16. Guo H, Yang J, Gallazzi F, Miao Y. Effects of the amino acid linkers on melanoma-targeting and pharmacokinetic properties of indium-111-labeled lactam bridge-cyclized α-MSH peptides. J. Nucl. Med 2011, 52, 608–616. [PubMed: 21421725]
17. Guo H, Gallazzi F, Miao Y. Design and evaluation of new Tc-99m-labeled lactam bridge-cyclized alpha-MSH peptides for melanoma imaging. Mol. Pharm 2013, 10, 1400–1408. [PubMed: 23418722]
18. Guo H, Miao Y. Introduction of an aminooctanoic acid linker enhances uptake of Tc-99m-labeled lactam bridge-cyclized alpha-MSH peptide in melanoma. J. Nucl. Med 2014, 55, 2057–2063. [PubMed: 25453052]
19. Guo H, Gallazzi F, Miao Y. Ga-67-labeled lactam bridge-cyclized alpha-MSH peptides with enhanced melanoma uptake and reduced renal uptake. Bioconjug. Chem 2012, 23, 1341–1348. [PubMed: 22621181]
20. Guo H, Miao Y. Cu-64-labeled lactam bridge-cyclized alpha-MSH peptides for PET imaging of melanoma. Mol. Pharm 2012, 9, 2322–2330. [PubMed: 22780870]
21. Guo H, Miao Y, Melanoma targeting property of a Lu-177-labeled lactam bridge-cyclized alpha-MSH peptide. Bioorg. Med. Chem. Lett 2013, 23, 2319–2323. [PubMed: 23473679]
22. Liu L, Xu J, Yang J, Feng C, Miao Y. Imaging human melanoma using a novel Tc-99m-labeled lactam bridge-cyclized alpha-MSH peptide. Bioorg. Med. Chem. Lett 2016, 26, 4724–4728. [PubMed: 27568083]
23. Yang J, Xu J, Gonzalez R, Lindner T, Kratochwil C, Miao Y. ^{68}Ga-DOTA-GGNle-CycMSH$_{hex}$ targets the melanocortin-1 receptor for melanoma imaging. Sci. Trans. Med 2018, 10, eaau4445.

24. Miao Y, Benwell K, Quinn TP. ^{99m}Tc and ^{111}In labeled alpha-melanocyte stimulating hormone peptides as imaging probes for primary and pulmonary metastatic melanoma detection. J. Nucl. Med 2007, 48, 73–80. [PubMed: 17204701]
25. Guo H, Yang J, Shenoy N, Miao Y. Gallium-67-labeled lactam bridge-cyclized alpha-melanocyte stimulating hormone peptide for primary and metastatic melanoma imaging. Bioconjug. Chem 2009, 20, 2356–2363. [PubMed: 19919057]
26. Miao Y, Shelton T, Quinn TP. Therapeutic efficacy of a ^{177}Lu labeled DOTA conjugated α-melanocyte stimulating hormone peptide in a murine melanoma-bearing mouse model. Cancer Biother. Radiopharm 2007, 22, 333–341. [PubMed: 17651039]
27. Raposinho PD, Correia JD, Alves S, Botelho MF, Santos AC, Santos I. A ^{99m}Tc(CO)$_3$-labeled pyrazolyl-α-melanocyte-stimulating hormone analog conjugate for melanoma targeting. Nucl. Med. Biol 2008, 35, 91–99. [PubMed: 18158948]
28. Morais M, Oliveira BL, Correia JD, Oliveira MC, Jiménez MA, Santos I, Raposinho PD. Influence of the bifunctional chelator on the pharmacokinetic properties of ^{99m}Tc(CO)$_3$-labeled cyclic α-melanocyte stimulating hormone analog. J. Med. Chem 2013, 56, 1961–1973. [PubMed: 23414214]
29. Jiang H, Kasten BB, Liu H, Qi S, Liu Y, Tian M, Barnes CL, Zhang H, Cheng Z, Benny PD. Novel, cysteine-modified chelation strategy for the incorporation of $[M^{I}(CO)_3]^+$ (M = Re/^{99m}Tc) in an α-MSH peptide. Bioconjug. Chem 2012, 23, 2300–2312. [PubMed: 23110503]
30. Kasten BB, Ma X, Liu H, Hayes TR, Barnes CL, Qi S, Cheng K, Bottorff SC, Slocumb WS, Wang J, Cheng Z, Benny PD. Clickable, hydrophilic ligand for *fac*-$[M^{I}(CO)_3]^+$ (M = Re/^{99m}Tc) applied in an *S*-functionalized α-MSH peptide. Bioconjug. Chem 2014, 25, 579–592. [PubMed: 24568284]
31. Miao Y, Figueroa SD, Fisher DR, Moore HA, Testa RF, Hoffman TJ, Quinn TP. ^{203}Pb-labeled α-melanocyte-stimulating hormone peptide as an imaging probe for melanoma detection. J. Nucl. Med 2008, 49, 823–829. [PubMed: 18413404]
32. Garmestani K, Milenic DE, Brady ED, Plascjak PS, Brechbiel MW. Purification of cyclotron-produced ^{203}Pb for labeling herceptin. Nucl. Med. Biol 2005, 32, 301–305. [PubMed: 15820766]
33. Máthé D, Szigeti K, Hegedűs N, Horváth I, Veres DS, Kovács B, Szűcs Z. Production and in vivo imaging of ^{203}Pb as a surrogate isotope for in vivo ^{212}Pb internal absorbed dose studies. Appl. Radiat. Isot 2016, 114, 1–6. [PubMed: 27156049]
34. Li M, Zhang X, Quinn TP, Lee D, Liu D, Kunkel F, Zimmerman BE, McAlister D, Olewein K, Menda Y, Mirzadeh S, Copping R, Johnson FL, Schultz MK. Automated cassette-based production of high specific activity [$^{203/212}$Pb] peptide-based theranostic radiopharmaceuticals for image-guided radionuclide therapy for cancer. Appl. Radiat. Isot 2017, 127, 52–60. [PubMed: 28521118]
35. Miao Y, Hylarides M, Fisher DR, Shelton T, Moore H, Wester DW, Fritzberg AR, Winkelmann CT, Hoffman TJ, Quinn TP. Melanoma therapy via peptide-targeted α-radiation. Clin. Cancer Res 2005, 11, 5616–5621. [PubMed: 16061880]

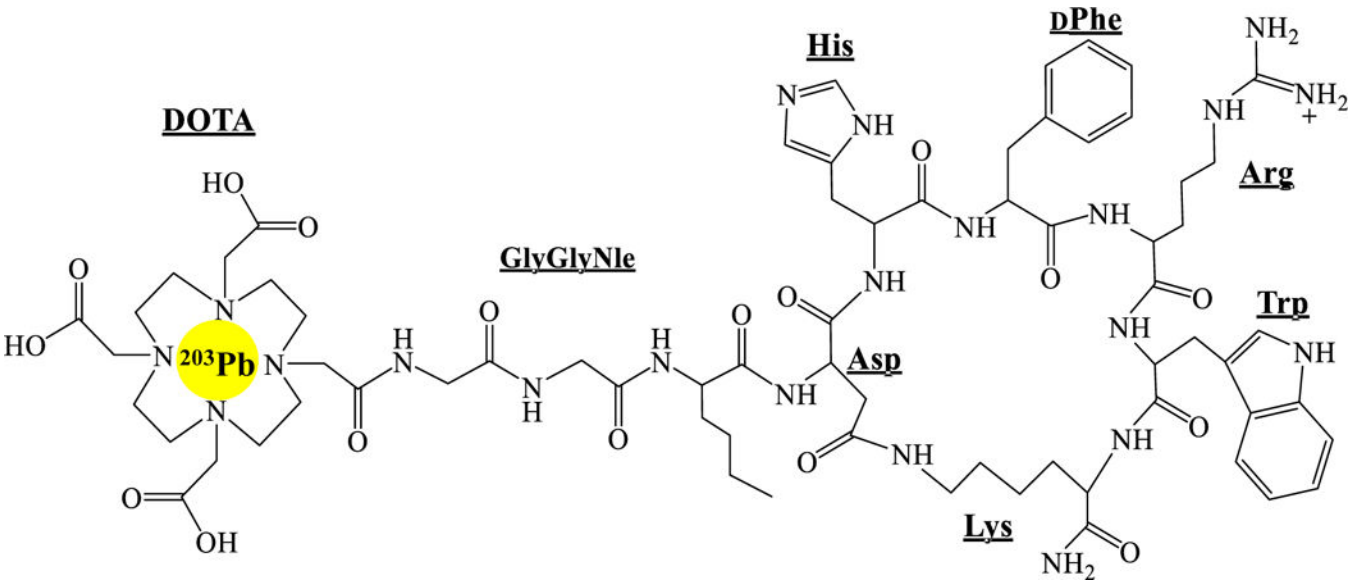

Figure 1.
Schematic structure of ^{203}Pb-DOTA-GGNle-CycMSH$_{hex}$.

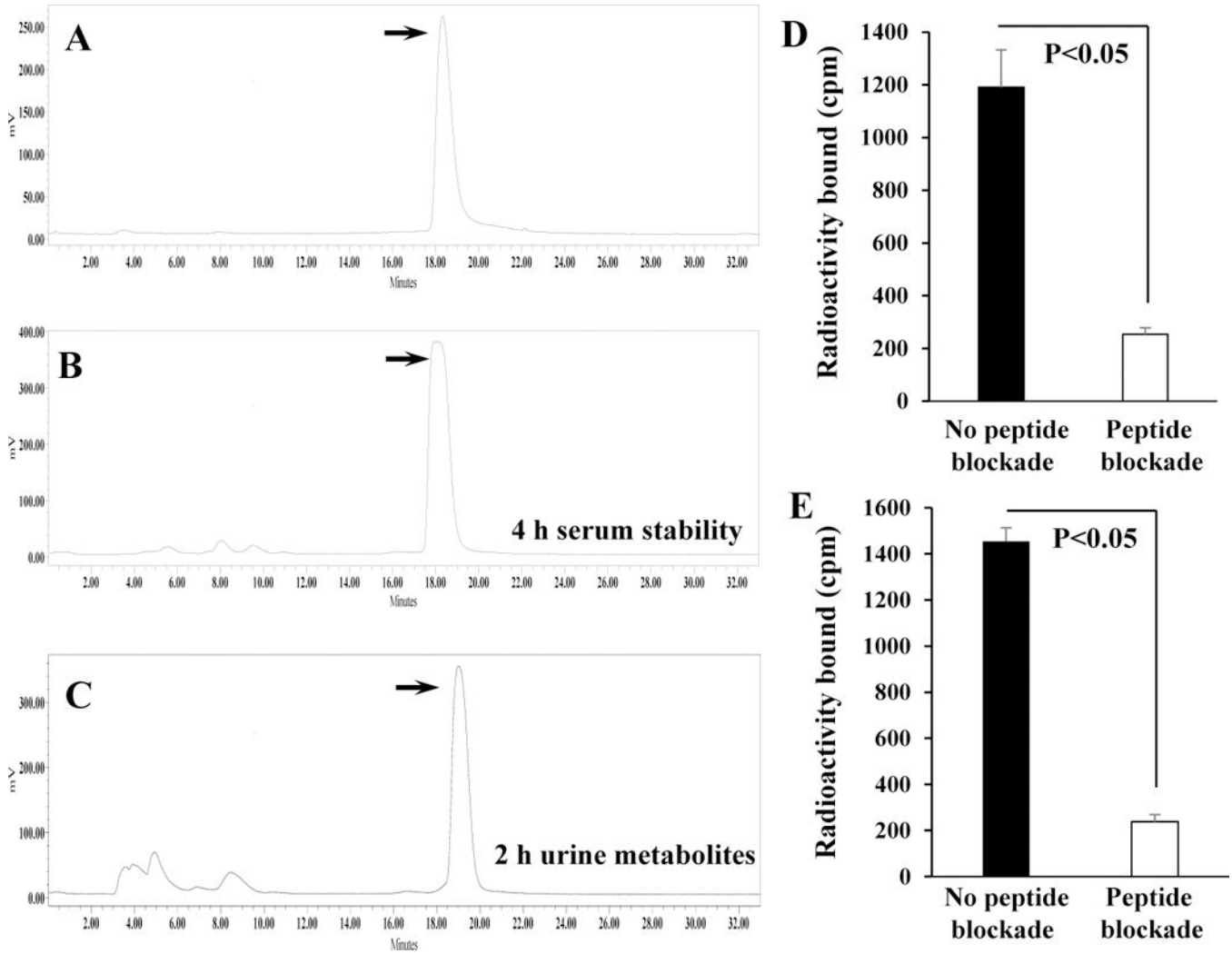

Figure 2.

Radioactive HPLC profile of ^{203}Pb-DOTA-GGNle-CycMSH$_{hex}$ (A, T_R = 18.3 min) and its mouse serum stability (B) after 4 h incubation at 37 °C. Radioactive HPLC profile of the urine sample of a normal C57 mouse at 2 h post-injection of ^{203}Pb-DOTA-GGNle-CycMSH$_{hex}$ (C). Arrows indicate the original compound of ^{203}Pb-DOTA-GGNle-CycMSH$_{hex}$. Specific binding of ^{203}Pb-DOTA-GGNle-CycMSH$_{hex}$ on B16/F1 (D) and B16/F10 (E) melanoma cells with or without peptide blockade.

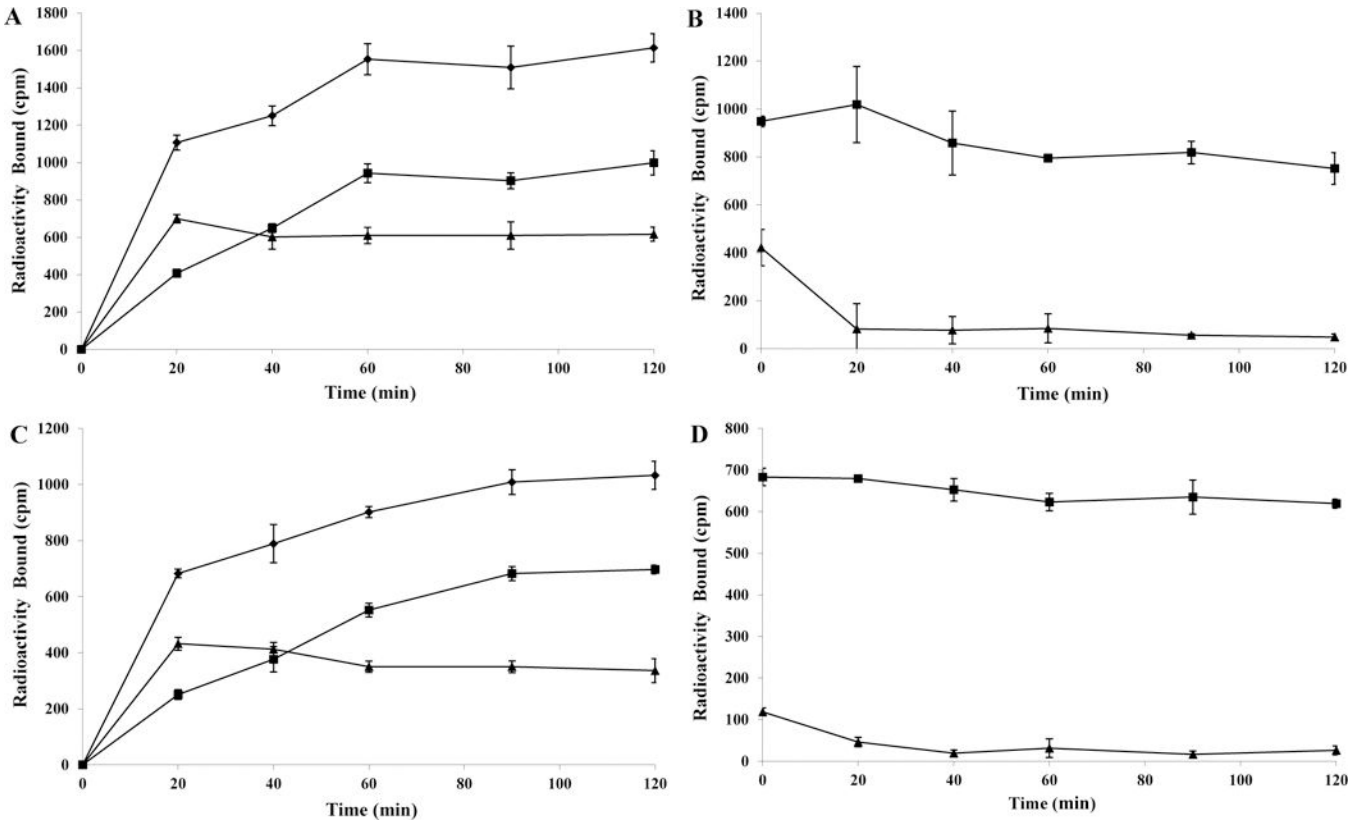

Figure 3.

Cellular internalization (A, C) and efflux (B, D) of ^{203}Pb-DOTA-GGNle-CycMSH$_{hex}$ on B16/F1 (A, B) and B16/F10 (C, D) melanoma cells. Total bound radioactivity (♦), internalized radioactivity (■) and cell membrane radioactivity (▲) are presented as counts per minute (cpm).

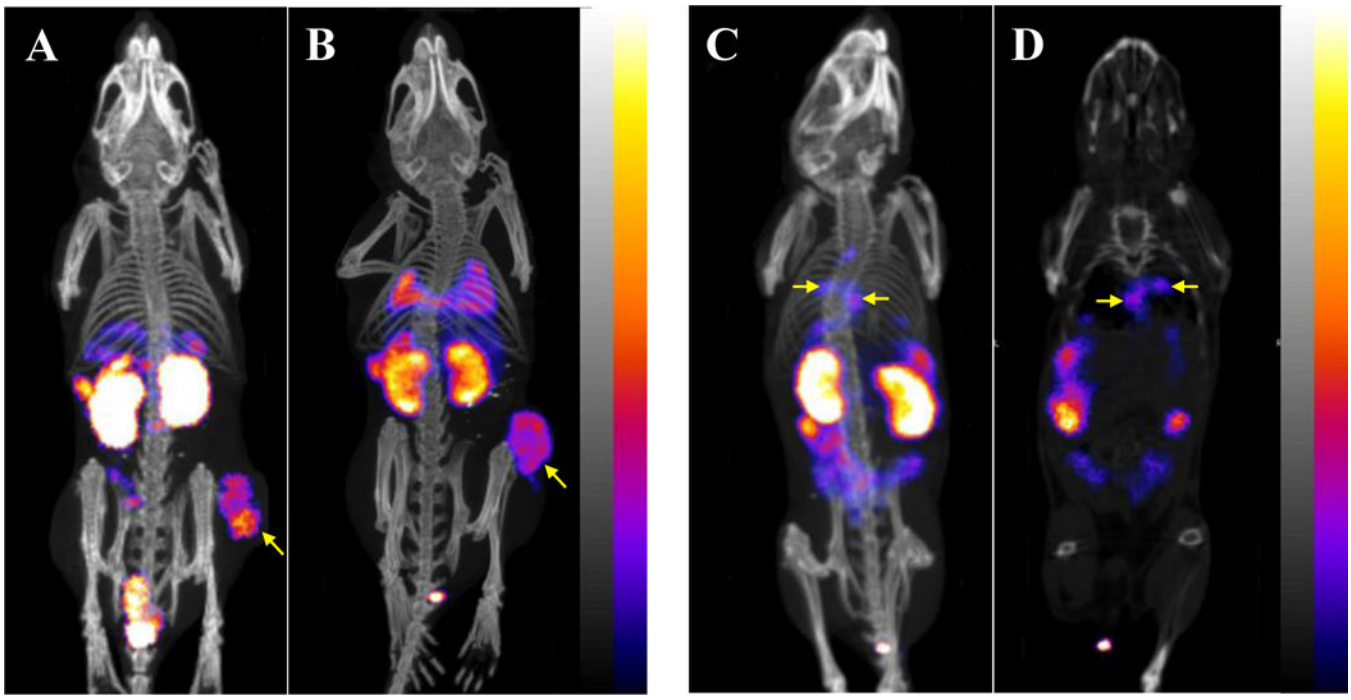

Figure 4.

Representative maximum intensity projection SPECT/CT images of B16/F1 (A) and B16/F10 (B) flank melanoma-bearing C57 mice, maximum intensity projection SPECT/CT and coronal images of B16/F10 pulmonary metastatic melanoma-bearing (C, D) C57 mice using ^{203}Pb-DOTA-GGNle-CycMSH$_{hex}$ as an imaging probe at 2 h post-injection.

Table 1.

Biodistribution of ^{203}Pb-DOTA-GGNle-CyCMSH$_{hex}$ in B16/F1 murine melanoma-bearing C57 mice. The data were presented as percent injected dose/gram or as percent injected dose (Mean ± SD, n = 5)

Tissues	0.5 h	2 h	2 h blockade	4 h	24 h
			Percent injected dose/gram (% ID/g)		
Tumor	14.37 ± 3.43	12.61 ± 2.28	0.68 ± 0.21*	9.37 ± 2.23	6.40 ± 0.37
Brain	0.11 ± 0.04	0.01 ± 0.01	0.01 ± 0.01	0.03 ± 0.02	0.01 ± 0.02
Blood	2.40 ± 0.57	0.25 ± 0.11	0.27 ± 0.12	0.14 ± 0.07	0.09 ± 0.04
Heart	1.0 ± 0.19	0.08 ± 0.09	0.11 ± 0.04	0.07 ± 0.07	0.02 ± 0.03
Lung	2.16 ± 0.29	0.27 ± 0.07	0.24 ± 0.15	0.18 ± 0.04	0.09 ± 0.02
Liver	1.08 ± 0.10	0.64 ± 0.11	0.61 ± 0.11	0.54 ± 0.08	0.52 ± 0.02
Skin	2.16 ± 0.79	0.12 ± 0.08	0.12 ± 0.17	0.11 ± 0.08	0.18 ± 0.13
Spleen	0.61 ± 0.22	0.15 ± 0.15	0.07 ± 0.12	0.13 ± 0.06	0.17 ± 0.10
Stomach	1.10 ± 0.37	0.97 ± 1.09	0.70 ± 0.53	0.49 ± 0.10	1.32 ± 0.49
Kidneys	9.3 ± 1.75	4.99 ± 1.48	4.61 ± 0.75	4.82 ± 0.59	2.77 ± 0.81
Muscle	0.38 ± 0.19	0.07 ± 0.09	0.01 ± 0.01	0.01 ± 0.01	0.01 ± 0.01
Pancreas	0.31 ± 0.18	0.05 ± 0.06	0.04 ± 0.04	0.01 ± 0.01	0.01 ± 0.01
Bone	1.17 ± 0.46	0.35 ± 0.34	0.20 ± 0.26	0.31 ± 0.27	0.46 ± 0.14
			Percent injected dose (% ID)		
Intestines	1.04 ± 0.13	1.25 ± 0.65	1.21 ± 0.52	2.13 ± 1.13	2.09 ± 1.56
Urine	78.62 ± 0.59	92.11 ± 3.55	94.25 ± 1.99	93.45 ± 1.0	94.45 ± 1.58
			Uptake ratio of tumor/normal tissue		
Tumor/blood	5.99	50.44	2.52	66.93	71.11
Tumor/kidney	1.55	2.53	0.15	1.94	2.31
Tumor/liver	6.65	46.70	2.83	52.06	71.11
Tumor/lung	13.31	19.70	1.11	17.35	12.31
Tumor/muscle	37.82	180.14	68.0	937.0	640.0

* $p<0.05$ for determining significance of differences in tumor and kidney uptake between ^{203}Pb-DOTA-GGNle-CyCMSH$_{hex}$ with or without peptide blockade at 2 h post-injection.

Table 2.

Biodistribution of ^{203}Pb-DOTA-GGNle-CyCMSH$_{hex}$ in B16/F10 murine melanoma-bearing C57 mice. The data were presented as percent injected dose/gram or as percent injected dose (Mean ± SD, n = 5)

Tissues	0.5 h	2 h	2 h blockade	4 h	24 h
			Percent injected dose/gram (% ID/g)		
Tumor	11.29 ± 4.42	16.81 ± 5.48	0.79 ± 0.50*	12.67 ± 1.48	4.57 ± 2.17
Brain	0.20 ± 0.06	0.03 ± 0.01	0.01 ± 0.02	0.04 ± 0.03	0.05 ± 0.05
Blood	3.31 ± 1.84	0.23 ± 0.06	0.15 ± 0.03	0.18 ± 0.07	0.38 ± 0.11
Heart	1.88 ± 0.89	0.13 ± 0.05	0.1 ± 0.05	0.09 ± 0.02	0.12 ± 0.05
Lung	3.61 ± 2.20	0.64 ± 0.16	0.62 ± 0.07	0.83 ± 0.13	0.26 ± 0.14
Liver	1.64 ± 0.39	0.77 ± 0.16	0.63 ± 0.02	0.71 ± 0.09	0.50 ± 0.16
Skin	3.16 ± 1.21	0.35 ± 0.16	0.40 ± 0.44	0.35 ± 0.24	0.38 ± 0.21
Spleen	0.87 ± 0.24	0.37 ± 0.09	0.14 ± 0.10	0.39 ± 0.11	0.37 ± 0.17
Stomach	1.58 ± 0.61	0.55 ± 0.12	0.18 ± 0.01	0.52 ± 0.13	0.16 ± 0.06
Kidneys	12.9 ± 4.98	5.43 ± 2.0	4.75 ± 0.48	5.31 ± 1.10	3.87 ± 2.12
Muscle	0.57 ± 0.12	0.21 ± 0.34	0.08 ± 0.09	0.12 ± 0.02	0.13 ± 0.10
Pancreas	0.56 ± 0.25	0.04 ± 0.07	0.04 ± 0.05	0.09 ± 0.07	0.17 ± 0.10
Bone	1.26 ± 0.48	0.38 ± 0.15	0.15 ± 0.13	0.37 ± 0.18	0.54 ± 0.26
			Percent injected dose (% ID)		
Intestines	1.25 ± 0.41	0.49 ± 0.08	0.39 ± 0.15	0.53 ± 0.15	0.30 ± 0.09
Urine	59.99 ± 8.23	80.5 ± 10.68	95.39 ± 1.15	89.71 ± 1.06	95.51 ± 1.85
			Uptake ratio of tumor/normal tissue		
Tumor/blood	3.41	73.09	5.27	70.39	12.03
Tumor/kidney	0.88	3.10	0.17	2.39	1.18
Tumor/liver	3.13	26.27	1.27	15.27	17.58
Tumor/lung	6.88	21.83	1.25	17.85	9.14
Tumor/muscle	19.81	80.05	9.88	105.58	35.15

*$p<0.05$ for determining significance of differences in tumor and kidney uptake between ^{203}Pb-DOTA-GGNle-CyCMSH$_{hex}$ with or without peptide blockade at 2 h post-injection.

Table 3.

Biodistribution of ^{203}Pb-DOTA-GGNle-CyCMSH$_{hex}$ in B16/F10 pulmonary metastatic melanoma-bearing and normal C57 mice. The data was presented as percent injected dose/gram or as percent injected dose (Mean ± SD, n = 3).

	2 h		4 h		24 h	
Tissues	**Lung Met.**	**Normal**	**Lung Met.**	**Normal**	**Lung Met.**	**Normal**
Percent injected dose/gram (% ID/g)						
Lung	7.32 ± 2.13*	0.42 ± 0.16	9.27 ± 1.13*	0.28 ± 0.15	3.90 ± 0.18*	0.29 ± 0.12
Brain	0.04 ± 0.02	0.05 ± 0.01	0.02 ± 0.01	0.04 ± 0.01	0.01 ± 0.01	0.01 ± 0.02
Blood	0.15 ± 0.04	0.72 ± 0.12	0.09 ± 0.04	0.59 ± 0.16	0.15 ± 0.10	0.30 ± 0.05
Heart	0.47 ± 0.46	0.27 ± 0.18	0.46 ± 0.28	0.28 ± 0.08	0.15 ± 0.07	0.16 ± 0.07
Liver	0.60 ± 0.05	1.03 ± 0.13	0.65 ± 0.06	1.08 ± 0.34	0.45 ± 0.09	1.04 ± 0.21
Skin	0.39 ± 0.05	0.27 ± 0.10	0.32 ± 0.15	0.22 ± 0.17	0.35 ± 0.05	0.17 ± 0.11
Spleen	0.25 ± 0.08	0.08 ± 0.09	0.24 ± 0.09	0.26 ± 0.20	0.24 ± 0.03	0.28 ± 0.11
Stomach	0.90 ± 0.49	0.55 ± 0.16	0.49 ± 0.13	0.53 ± 0.20	0.32 ± 0.16	1.67 ± 0.93
Kidneys	8.13 ± 3.29	5.84 ± 2.86	6.16 ± 0.31	6.66 ± 1.26	3.55 ± 0.36	4.48 ± 1.14
Muscle	0.04 ± 0.05	0.08 ± 0.08	0.08 ± 0.06	0.01 ± 0.01	0.09 ± 0.10	0.06 ± 0.05
Pancreas	0.01 ± 0.01	0.16 ± 0.12	0.05 ± 0.01	0.07 ± 0.11	0.09 ± 0.01	0.09 ± 0.03
Bone	0.13 ± 0.08	1.15 ± 0.36	0.15 ± 0.08	0.77 ± 0.35	0.31 ± 0.24	1.06 ± 0.54
Percent injected dose (% ID)						
Intestine	0.61 ± 0.52	1.43 ± 0.58	1.66 ± 1.49	1.68 ± 0.96	0.76 ± 0.57	1.86 ± 1.02
Urine	90.66 ± 1.33	83.92 ± 11.77	88.45 ± 1.9	92.02 ± 2.16	93.18 ± 1.47	92.07 ± 2.14

*$p<0.05$, significance comparison between ^{203}Pb-DOTA-GGNle-CycMSH$_{hex}$ in pulmonary metastatic melanoma-bearing and normal C57 mice.